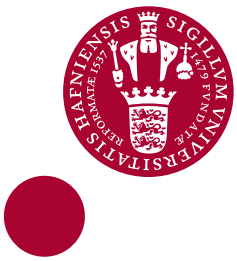

Feasibility of simultaneous PET/MR of the carotid artery: first clinical experience and comparison to PET/CT

Ripa, Rasmus Sejersten; Knudsen, Andreas; Hag, Anne Mette Fisker; Lebech, Anne-Mette; Loft, Annika; Keller, Sune Høgild; Hansen, Adam Espe; von Benzon, Eric; Højgaard, Liselotte; Kjær, Andreas

Published in:
American Journal of Nuclear Medicine and Molecular Imaging

Publication date:
2013

Document version
Publisher's PDF, also known as Version of record

Am J Nucl Med Mol Imaging 2013;3(4):361-371
www.ajnmmi.us /ISSN:2160-8407/ajnmmi1305002

Original Article

Feasibility of simultaneous PET/MR of the carotid artery: first clinical experience and comparison to PET/CT

Rasmus S Ripa[1,3], Andreas Knudsen[1,2], Anne Mette F Hag[1], Anne-Mette Lebech[2], Annika Loft[1], Sune H Keller[1], Adam E Hansen[1], Eric von Benzon[1], Liselotte Højgaard[1], Andreas Kjær[1]

[1]Department of Clinical Physiology, Nuclear Medicine and PET, Rigshopitalet University Hospital & Cluster for Molecular Imaging, Faculty of Health and Medical Sciences, University of Copenhagen, Copenhagen, Denmark; [2]Department of Infectious Diseases, Hvidovre University Hospital, Denmark; [3]Department of Clinical Physiology and Nuclear Medicine, Bispebjerg University Hospital, Denmark

Received May 26, 2013; Accepted June 20, 2013; Epub July 10, 2013; Published July 15, 2013

Abstract: The study aimed at comparing PET/MR to PET/CT for imaging the carotid arteries in patients with known increased risk of atherosclerosis. Six HIV-positive men underwent sequential PET/MR and PET/CT of the carotid arteries after injection of 400 MBq of ^{18}F-FDG. PET/MR was performed a median of 131 min after injection. Subsequently, PET/CT was performed. Regions of interest (ROI) were drawn slice by slice to include the carotid arteries and standardized uptake values (SUV) were calculated from both datasets independently. Quantitative comparison of ^{18}F-FDG uptake revealed a high congruence between PET data acquired using the PET/MR system compared to the PET/CT system. The mean difference for SUV_{mean} was -0.18 ($p < 0.001$) and -0.14 for SUV_{max} ($p < 0.001$) indicating a small but significant bias towards lower values using the PET/MR system. The 95% limits of agreement were -0.55 to 0.20 for SUV_{mean} and -0.93 to 0.65 for SUV_{max}. The image quality of the PET/MR allowed for delineation of the carotid vessel wall. The correlations between ^{18}F-FDG uptake from ROI including both vessel wall and vessel lumen to ROI including only the wall were strong ($r = 0.98$ for SUV_{mean} and $r = 1.00$ for SUV_{max}) indicating that the luminal ^{18}F-FDG content had minimal influence on the values. The study shows for the first time that simultaneous PET/MR of the carotid arteries is feasible in patients with increased risk of atherosclerosis. Quantification of ^{18}F-FDG uptake correlated well between PET/MR and PET/CT despite difference in method of PET attenuation correction, reconstruction algorithm, and detector technology.

Keywords: Atherosclerosis, positron emission tomography, magnetic resonance imaging, PET/MR, hybrid scanners

Introduction

Atherosclerosis usually remains asymptomatic until it has reached an advanced phase. Therefore methods for non-invasive identification of both early and very advanced atherosclerotic plaques are pursued. The use of ^{18}F-FDG positron emission tomography (PET) or magnetic resonance (MR) for imaging atherosclerosis has received much attention recently. ^{18}F-FDG PET has been used as a molecular marker of inflammation and thus perhaps vulnerability of plaques [1, 2] and MR imaging has been proven effective in differentiating plaque components based on signal intensities and morphological appearance of the plaque on different imaging sequences [3, 4]. In addition, two recent studies have found an increase in FDG uptake in the carotid artery of HIV-positive patients without any symptoms of cardiovascular disease [5, 6]. Since HIV-positive patients are known to have an increased risk of atherosclerosis, it has been speculated that the increase in FDG uptake could be a marker of very early atherosclerotic changes (e.g. endothelial dysfunction). Combined MR and PET can be expected to have an added value over PET/CT in non-invasive imaging of atherosclerosis [7] since CT in essence does not visualize the vessel wall but primarily the lumen.

Recently, a whole-body PET/MR imager was developed that allows simultaneous MR and

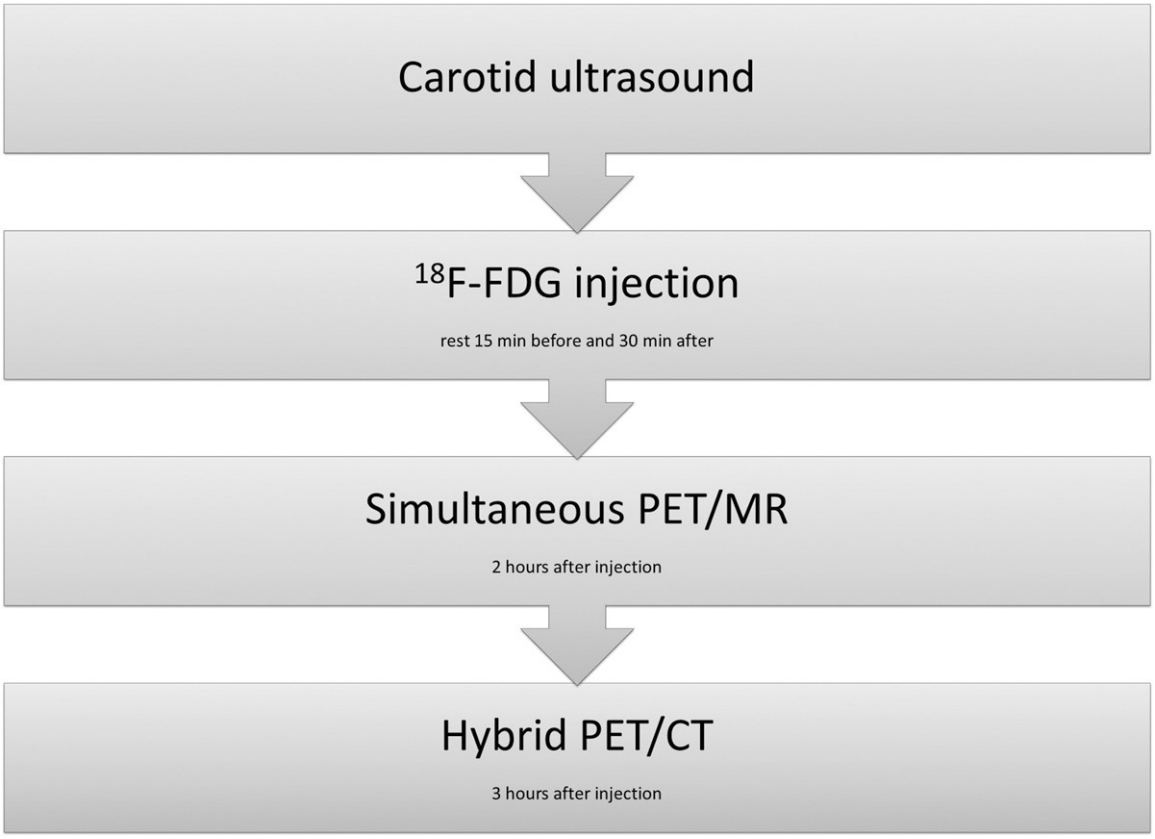

Figure 1. Flow chart of the study.

PET imaging. The machine (Biograph mMR) consists of a 3-Tesla MR scanner that encloses an avalanche photodiode–based PET system within its gantry. The main advantage of the simultaneous isocentric acquisition when imaging atherosclerosis is the perfect alignment between PET and MR allowing for a precisedelineation of the vessel wall or plaque and characterization of subareas of a plaque (e.g. the necrotic core) along with decreased examination time compared to sequential MR and PET. In comparison with PET/CT the advantages are decreased radiation and superior soft-tissue characterization with MR. However, the quality of the acquired PET and MR data may be affected in a combined PET/MR system. First, the attenuation correction of the PET data has to be derived from MR information. This is problematic since MR does not contain direct information about the attenuation from the tissue. Second, the PET detectors inside the MR scanner cause inhomogeneities in the magnetic field and electromagnetic interference, which potentially degrade the MR image quality. Finally, the replacement of the photomultipliers with avalanche photodiodes may affect the PET acquisition.

So far, the quality of clinical PET examinations from integrated whole-body PET/MR scanners with attenuation correction using MR data have only been systematically compared with examinations acquired on a PET/CT scanner in the same patients in very few trials [8, 9]. These studies found the reliability of PET/MR to be comparable to that of PET/CT in the detection of lesions suspicious for malignancy. Another recent phantom experiment did not find any perceptible impact on the overall performance of the system [10]. Imaging the carotid arteries with the PET/MR system has so far never been published in humans.

The aim of this study was for the first time to evaluate the feasibility of integrated PET/MR imaging of the carotid arteries in humans by: 1) comparison of the standardized uptake value (SUV) in the carotid arteries obtained with integrated PET/MR with SUV from PET/CT in the same HIV-positive patients. 2) Comparison of SUV obtained when including only the vessel

wall in the region of interest (ROI), with the traditional approach of including both vessel wall and lumen in the ROI.

Materials and methods

Study design

Six HIV-positive patients were prospectively recruited at routine visits at our outpatient clinic. Inclusion criteria were i) HIV infected, ii) age 18-70 years and iii) receiving cART > 12 months.

Exclusion criteria were symptoms of cardiovascular disease, age < 18 years, diabetes, pregnancy, renal insufficiency, treatment with cholesterol lowering drugs, or severe claustrophobia.

All patients underwent a single-injection dual-imaging protocol of simultaneous PET/MR and subsequent integrated PET/CT on the same day. PET/MR and PET/CT was performed with less than 1 hour (range 35 to 49 minutes) between the two PET acquisitions using the same ^{18}F-FDG injection. On the same day (before tracer injection) real-time intima media thickness was measured in the common carotid artery 1 cm caudal of the *bulbus arteriosus* (RF-QIMT, Esaote, Italy). An outline of the study design is shown in **Figure 1**.

Patients fasted at least 6 hours prior to injection of 400 MBq ^{18}F-FDG (range 397-405) in a cubital vein catheter. Plasma glucose measured before injection ranged from 4.0 to 6.0 mmol/l. To reduce tracer uptake in neck and mouth musculature the patients were not allowed to talk and to avoid uptake in brown fat they rested in calm and warm surroundings from 15 min before injection until 30 min after injection.

Ethical approval

The study was approved by the Regional Scientific Ethical Committee (protocol H-4-2010-044) and all subjects received oral and written information about the study and signed an informed consent before inclusion.

PET/MR acquisition

Simultaneous PET/MR was performed on the Biograph mMR (Siemens Healtcare) using a dedicated head and neck coil (Siemens Healthcare). Patients were fixed in the scanner and imaging started a median of 131 minutes after ^{18}F-FDG injection. Scout images were obtained for localization of the carotid arteries. An mMR standard Dixon water-fat MR sequence was then recorded and segmented (into air, lung tissue, soft tissue and fat) for MR-based PET attenuation correction (MR-AC) [11]. A 3D time-of-flight (TOF) bright magnetic resonance angiography sequence was then performed to obtain lumen contours. MR parameters for 3D-TOF were: TR/TE 21/3.6 ms, flip angle 12°.

Next, a stack of 14 axial 2D turbo spin echo dark blood images with fat suppression of the common carotid arteries in proton density, T1 and T2 weightings with slice thickness of 2 mm and matrix size of 256 were centered using the 3D-TOF angiography. Images were centered with 4 slices cranial to the bifurcation on the right side, and 10 slices caudal to the bifurcation. MR parameters were: T1-weighted: double inversion recovery, TR/TE = 1060/26 ms, echo train length = 7. T2-weighted: TR/TE = 2500/76 ms, echo train length = 15. Proton density-weighted: TR/TE = 2400/16 ms, echo train length = 15.

PET acquisition was started simultaneously with the start of the Dixon MR sequence using the same bed position. Acquisition time was 10 min in three-dimensional list mode. The total average examination time was below 30 minutes.

PET/CT acquisition

Three hours after ^{18}F-FDG injection (range 166 to 181 minutes), the patient was scanned using a combined PET/CT-scanner (Siemens Biograph mCT64, Siemens, Berlin, Germany). PET was acquired in three-dimensional list mode for 3 min over one field of view centered at the carotid bifurcation. Two CT examinations were performed in each patient; one CT scan (120 kV, reference mAs 225 (care dose)) for attenuation correction preceded the PET acquisition and one contrast enhanced CT scan (120 kV, reference mAs 225 (care dose)) was performed just after the PET acquisition. Contrast was injected by pump (100 ml of Optiray 300 mg/ml at 2.5 ml/s followed by 100 ml of saline at 2.5 ml/s) and the CT was automatically initiated after a delay of 10 s when a cutoff of 80 Hounsfield units was reached in the descending aorta.

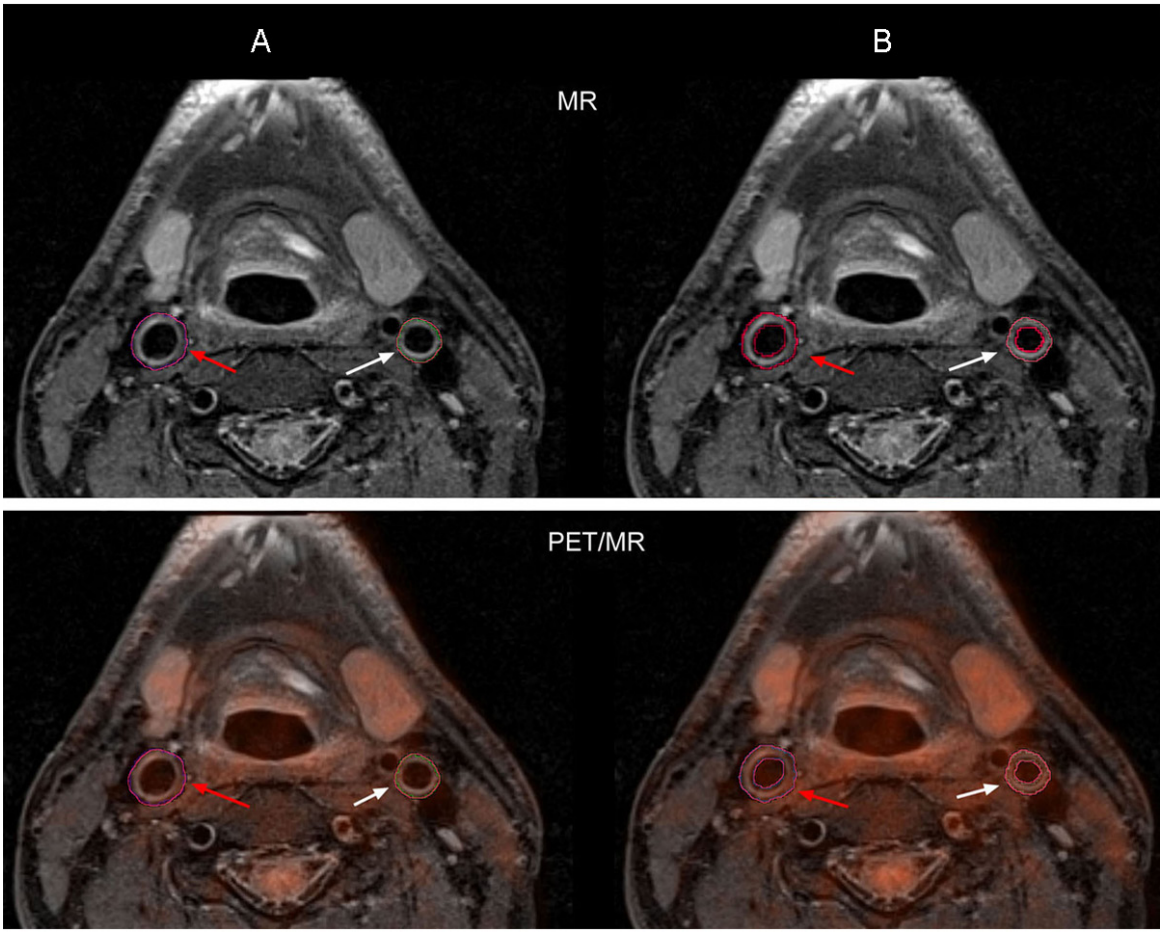

Figure 2. MR and fused FDG-PET/MR. Example of transverse MR and fused FDG-PET/MR (same patient and slice position as Figure 3) at a level with the right common carotid artery (red arrow) and the left internal carotid artery (white arrow). A ROI including both the vessel wall and lumen is drawn in column A, and a ROI including only the vessel wall is drawn in column B.

Image reconstruction

All patients had 2 PET datasets of the carotid artery; "PET/MR" from the PET/MR system with parameters optimized for the PET/MR system and "PET/CT" from the PET/CT system reconstructed with parameters optimized for the PET/CT system. The PET from the PET/MR scan was reconstructed using ordered-subsets expectation maximization iterative reconstruction algorithm (OSEM 3D) (6 iterations, 21 subsets, zoom 2.0) with MR based attenuation correction yielding 512 x 512 image slices (voxel size: 0.70 x 0.70 x 2.03 mm). Attenuation maps for correction of the PET data from the PET/MR scanner were generated on the basis of the Dixon water-fat MR sequence [11]. This procedure operates automatically in the postprocessing software of the scanner.

PET/CT: A routinely used, optimized clinical reconstruction setting using CT based attenuation correction [1] was used on the PET from the PET/CT, using both resolution-recovery (point spread function, TrueX) and time-of-flight (2 iterations, 21 subsets, zoom 1.0) giving 400 x 400 image slices (voxel size 2.04 x 2.04 x 2.00). A 2 mm full width at half maximum Gaussian filter was the applied to all images post-reconstruction.

Data analysis

Anatomical co-registration of CT and MR was done by automatic rigid registration and subsequent visual confirmation of anatomical landmarks like the carotid bifurcation and the vertebral arteries. The carotid artery was analyzed slice by slice in every subject in the PET/CT

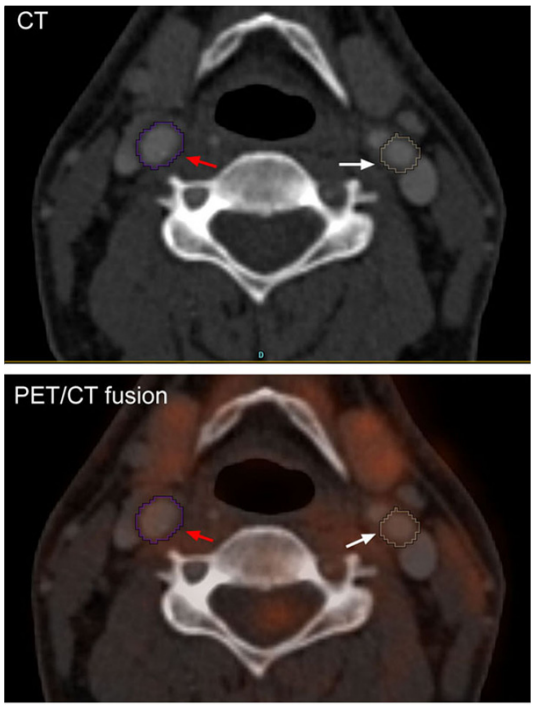

Figure 3. CT and fused FDG-PET/CT. Example of transverse CT and fused FDG-PET/CT from the same patient and slice position as Figure 2. The right common carotid artery is marked by a red arrow on the left internal carotid artery is marked by a white arrow. A ROI including both the vessel wall and lumen is drawn.

dataset and the PET/MR dataset independently. Dataset "PET/MR" was fused with the simultaneously acquired MR images (T1, T2, and proton density weighted). A free-hand ROI was drawn around the common carotid artery and the internal carotid artery slice by slice on the axial MR images including both the vessel wall and the vessel lumen (**Figure 2A**). All three MR weighted images were used in defining the vessel. SUV_{mean} and SUV_{max} that correct for injected dose, patient weight and time to acquisition were calculated for each ROI. Subsequently a similar approach was used on datasets "PET/CT" using only the contrast enhanced CT to identify the carotid artery and not the MR images (**Figure 3**).

Finally, new free-hand ROIs were drawn on the axial MR images including only the vessel wall and excluding the vessel lumen (**Figure 2B**). Again SUV_{mean} and SUV_{max} from these ROIs were calculated from dataset "PET/MR" on a slice by slice basis.

In summary, the data analysis resulted in 3 SUV_{mean} and 3 SUV_{max} calculations per slice, as well as 3 SUV_{mean} and 3 SUV_{max} calculations per artery (right/left).

Statistical analysis

SUV calculated from the PET/MR was compared with SUV calculated from the PET/CT using the method of Bland and Altman [12]. According to this method, the mean difference between measurements is defined as "bias" and represents the systemic error in measurements. The statistical significance of the bias was assessed using the t-test. The 95% limits of agreement were defined as mean difference ± 1.96 times the standard deviation. All limits of agreement were calculated assuming normal distribution of the differences. The agreement was further assessed using the Pearson r correlation coefficient. Comparisons were done both slice by slice (168 comparisons) and artery by artery (12 comparisons). Paired comparison of ROIs including or excluding the vessel lumen from SUV calculations were performed with the t-test. Analyses were performed with IBM SPSS Statistics (version 20, IBM).

Results

Patient characteristics are shown in **Table 1**. All patients were HIV-positive men on stable antiviral therapy. No patients had symptoms of cardiovascular disease, but one patient had an asymptomatic, stable aortic aneurism. The patients had only few classic cardiovascular risk factors. None of the patients had hemodynamic significant stenoses of the carotid arteries by the ultrasound. PET/MR and PET/CT examinations were feasible in all patients and all slices were analyzable. **Figure 4** shows an example of the four image sequences used for the MR examination with high luminal and external contrast of the carotid artery which are shown with arrows.

Quantitative comparison between PET obtained in the PET/MR scanner and in the PET/CT scanner

A total of 168 carotid vessel segments were analyzed with 14 axial slices per vessel.

SUV_{mean} and SUV_{max} were calculated from ROIs drawn independently using the PET/CT dataset only (**Figure 3**) or the PET/MR dataset only

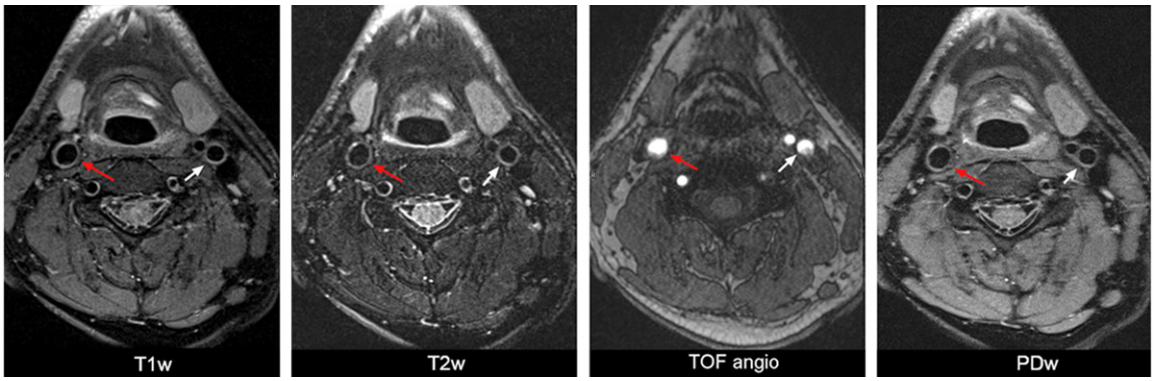

Figure 4. Example of 4 MR imaging sequences from identical location in the same patient. Images are T1 weighted (T1w), T2 weighted (T2w), Time of flight angiography (TOF angio) and proton density weighted (PDw). The vessel wall of the right common carotid artery (red arrow) and the left internal carotid artery (white arrow) appear hyperintense on T1w, T2w, and PDw images.

Table 1. Characteristics of the 6 included patients

	N
Male gender	6 (100%)
Age (median, range)	42 (29-66)
BMI (median, range)	25 (22-28)
Family history of ischemic heart disease	0
Smoking (current/ex/never)	0/1/0
Known hypertension	1 (17%)
Diabetes	0
Known cardiovascular disease	1 (17%)
Intima media thickness, μm (median, range)	672 (553-956)

(**Figure 2A**). The SUV_{max} ranged from 0.9 to 2.7 in the PET/MR system and from 1.1 to 3.2 in PET/CT system. The SUV_{mean} ranged from 0.5 to 1.8 and 0.8 to 2.1 in the PET/MR and PET/CT systems, respectively.

Values obtained by the two systems (PET/MR and PET/CT) were very similar (**Figures 5** and **6**) with a small but statistical significant bias (mean difference) of less than -0.2 ($p < 0.001$ for both SUV_{mean} and SUV_{max}). The bias was towards SUV from the PET/MR system being slightly lower than values from the PET/CT system. No extreme or outlying observations were found. The 95% limits of agreement were -0.6 to 0.2 for SUV_{mean} and -0.9 to 0.7 for SUV_{max} using the slice by slice comparison and -0.4 to 0.1 for SUV_{mean} and -0.6 to 0.4 for SUV_{max} using the vessel by vessel comparison. The correlations between the two systems were similarly high (**Figures 5** and **6**). The Bland-Altman plots of difference indicate that the variability of the difference between the systems is independent of the SUV magnitude. Also, the correlation between the two systems were moderate with the best correlation in the vessel by vessel comparisons for both SUV_{mean} (**Figure 5D**) and SUV_{max} (**Figure 6D**).

Comparison SUV with and without lumen

The luminal contributions to SUV_{mean} and SUV_{max} were minimal as shown by the almost perfect correlation between values obtained from an ROI including both vessel wall and lumen compared to including only the vessel wall from the simultaneous PET/MR examination (**Figures 2** and **7**). A total of 162 of the 168 slices (96%) had a perfect match (difference of 0.0) of SUV_{max} and 125 (74%) had a perfect match of SUV_{mean}. The mean increase in SUV_{mean} when excluding the vessel lumen compared to including the lumen in the ROI was 1.0% ($p = 0.002$) with a 95% confidence interval from 0.3% to 1.6%. In comparison, the mean increase in SUV_{max} was only 0.3% ($p = 0.02$) with 95% confidence interval from 0.04 to 0.5%.

Discussion

In this study of HIV patients with increased risk of atherosclerosis but without any symptoms of cardiovascular disease, we present the first results from simultaneous PET/MR of the carotid arteries. We found a high congruence between PET data acquired using PET/MR to identify the carotid artery and PET data acquired using traditional PET/CT to identify

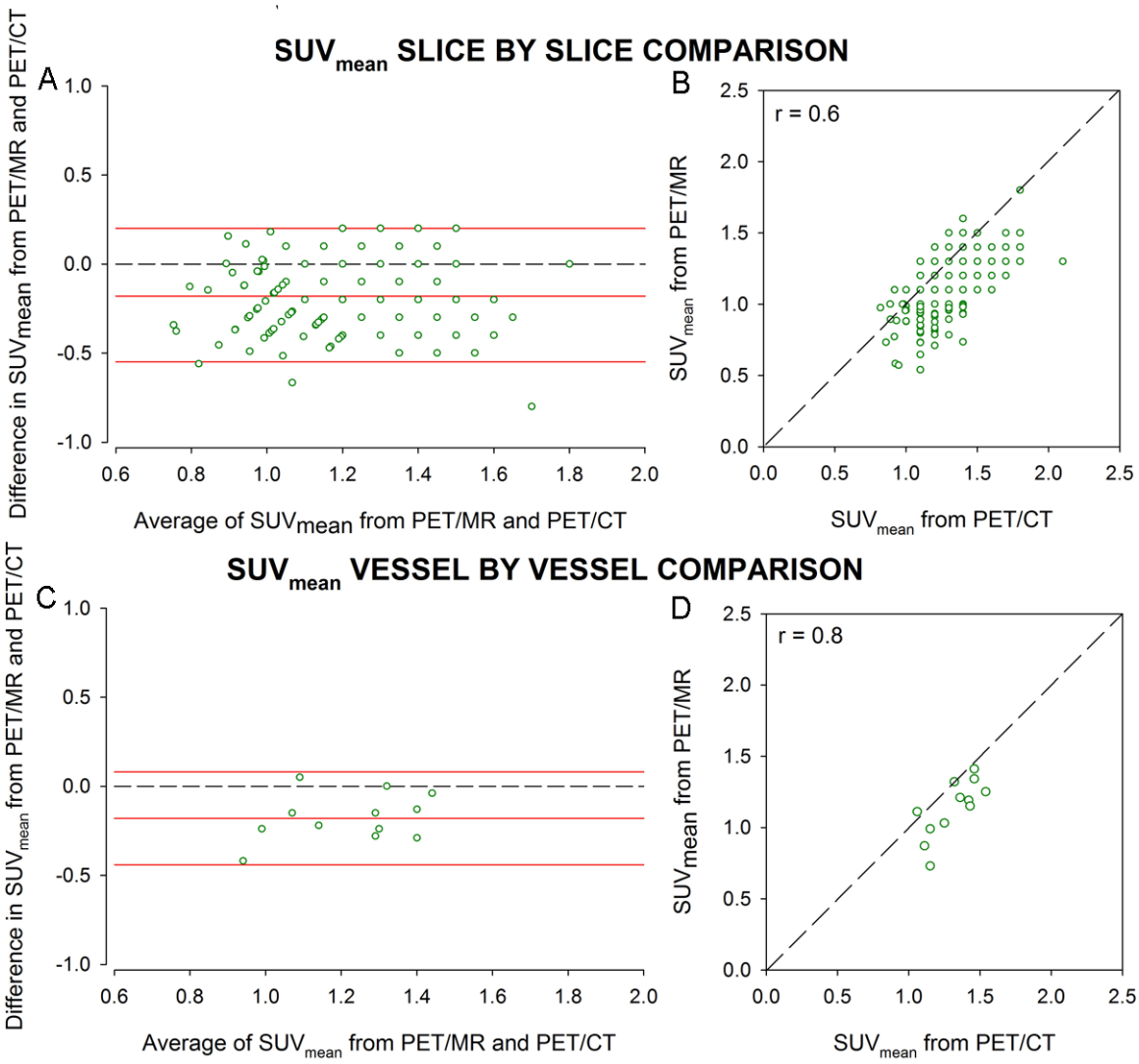

Figure 5. SUV_{mean} comparison between the PET/CT dataset and the PET/MR dataset. Slice by slice (n = 168, A and B) and vessel by vessel (n = 12, C and D). Panel A and C show the Bland-Altman plots of difference with identity line shown in black and the mean difference with 95% limits of agreement shown in horizontal red lines. Panel B and D show the correlation with a dashed black identity line.

the carotid artery indicating feasibility of simultaneous PET/MR for studies of the carotid arteries. Additionally, we found evidence that MR can be used to delineate both the inner and outer wall of the carotid artery and thus the possibility for a more specific ROI to calculate SUV from the fused PET acquisition.

Despite the obvious potential for synergy between PET and MR imaging in atherosclerosis, only a few human studies have applied these two modalities [7, 13, 14] and none have included patients with only mild atherosclerosis/endothelial dysfunction. This is probably at least in part caused by the very cumbersome process of anatomical alignment between MR and PET when acquired on separate standalone systems. In addition, it is very difficult to place the patient at the same position in the scanner with identical angulation of the neck required for perfect anatomical co-localization of the PET and the MR examination. The introduction of the hybrid PET/MR system overcomes these limitations and is thus a very suitable method for carotid artery imaging. However, the hybrid PET/MR system has other potential problems that need to be addressed. First, attenuation correction of the PET data is essential to gain accurate measurements. In PET/CT scanners, attenuation correction is

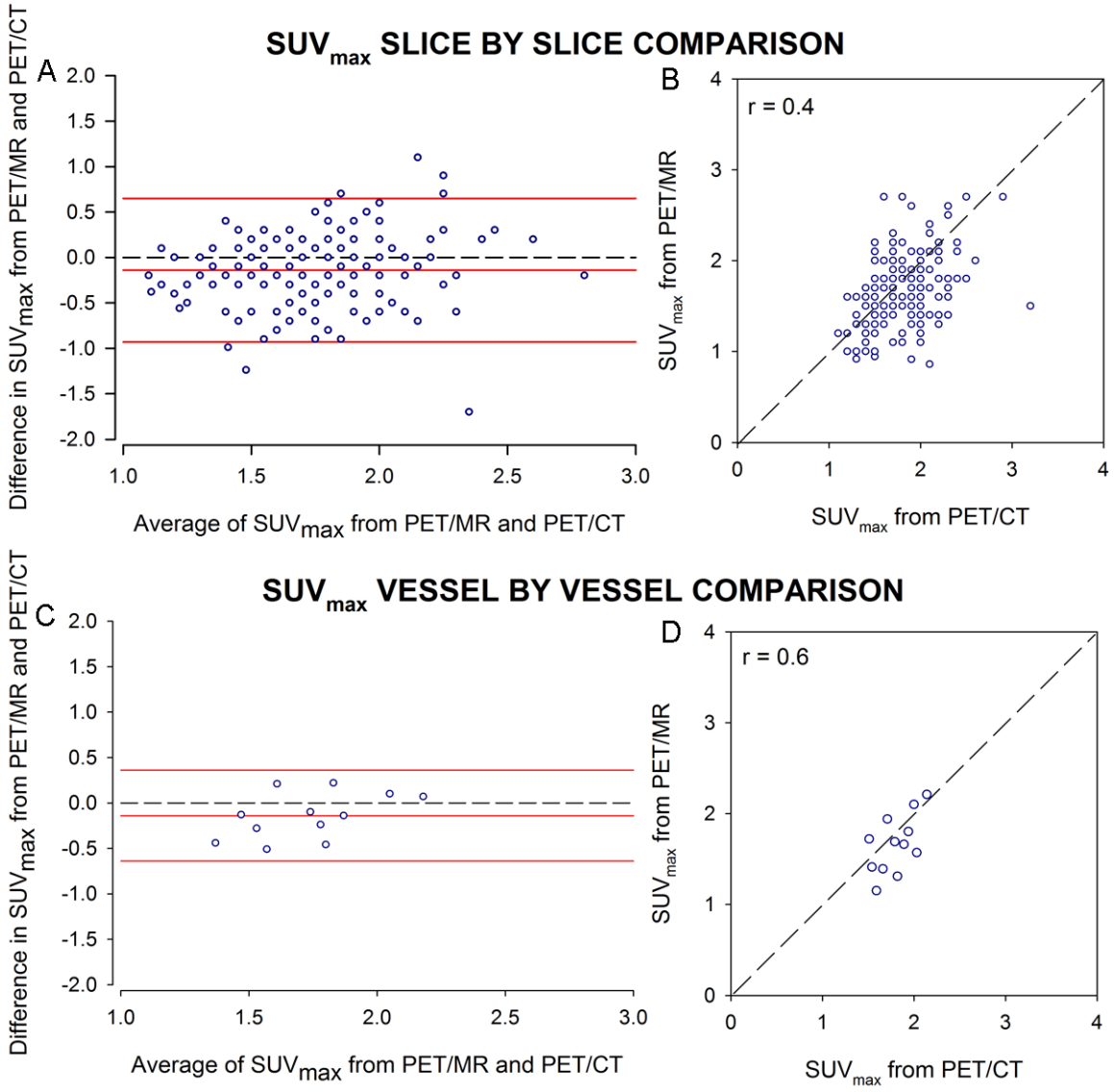

Figure 6. SUV_{max} comparison between the PET/CT dataset and the PET/MR dataset. Slice by slice (n = 168, A and B) and vessel by vessel (n = 12, C and D). Panel A and C show the Bland-Altman plots of difference with identity line shown in black and the mean difference with 95% limits of agreement shown in horizontal red lines. Panel B and D show the correlation with a dashed black identity line.

based on an accurate attenuation map generated from a CT transmission scan.

In MR, the image formation is based on nuclear magnetic resonance of the tissue which cannot directly be used for attenuation correction. Both available whole-body integrated PET/MR systems (Siemens mMR [10] and Philips Ingenuity TF [15]) uses segmentation of dedicated MR images for attenuation correction [11]. The estimated distribution of air, lungs, fat, and soft tissue (Siemens mMR) or air, lungs, and soft tissue (Philips Ingenuity TF) generates an attenuation map based on the presumed density of these tissue types. The obtained attenuation maps are without bone which can seriously affect the quantification of the PET images [16, 17]. Methods that in different ways include bones in MR-based attenuation maps are being developed [18-20] but are not yet available in any of the systems for clinical use. The impact of using Dixon MR-based attenuation correction with missing bones is estimated to give only a 4 ± 2% (mean ± SD) error on neck lesions [11] but no large scale studies or investigations specific to the neck region have been

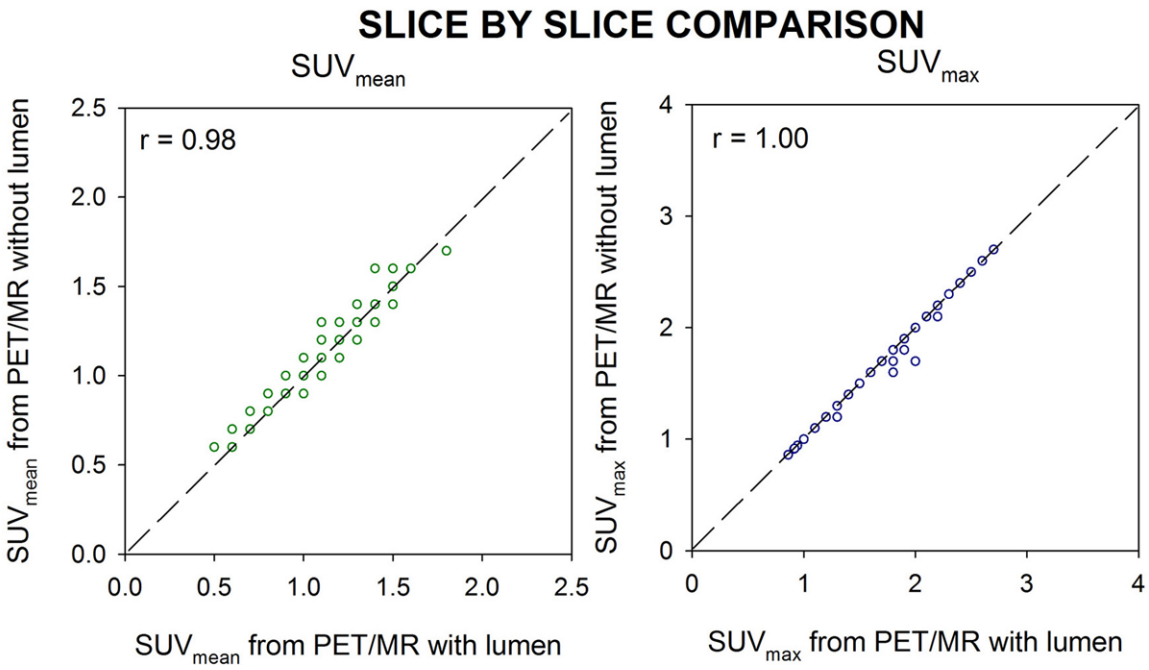

Figure 7. Correlation between SUV. SUV calculated from ROIs including only the vessel wall (Figure 2A) compared to ROIs including both vessel wall and vessel lumen (Figure 2B) using the same PET/MR images.

done. Our data support the hypothesis, that MR based attenuation correction of the carotid arteries are feasible since we find only a small mean difference (bias) and a strong correlation between SUV from the PET/MR system compared to SUV from the PET/CT system in the same patients. This further supports the recent findings of only small, but significant difference between SUV_{mean} in a number of organs in 32 patients with oncologic disease undergoing both PET/CT and subsequent simultaneous PET/MR [8].

The hypothesis of our trial was that we would find differences in SUV between the two systems since the ROIs including the carotid arteries would differ when using the CT or the MR images to delineate the vessel wall. It is clear from **Figure 4** that MR allows for superior delineation of especially the outer edge of the vessel as compared to the CT and it was our hypothesis that the PET/MR would give a more accurate calculation of the ^{18}F-FDG accumulation in the vessel wall than the PET/CT. Thus, even though the limits of agreement between the systems in our study are narrow, they could be of importance. Future studies comparing the two PET acquisitions to other measures of vessel inflammation or endothelial dysfunction such as histology or gene expression analysis are needed to determine any extra diagnostic information in the PET from the PET/MR compared to the PET from the PET/CT.

Methodological differences could also explain the difference in the SUVs observed. First, PET/MR and PET/CT were acquired with approximately 1 hour difference, however based on our previous comparison of SUV_{max} in the carotid artery after 1 hour and 3 hours, we find it unlikely that this time difference would have substantial effect on the results [21]. Second, the two PET scanners differ in both hardware (detector technology, geometry, presence of MR coils) and software (method of attenuation correction, time of flight, resolution-recovery) resulting in multiple reasons for variation in SUV as previously described [22].

The use of simultaneous PET/MR allow for precise delineation of both the inner and outer carotid vessel wall using the different weighted MR images. This could potentially lead to a more specific assessment of FDG accumulation in the vessel wall as compared to the conventional ROI including both vessel wall and lumen especially in patient without large atherosclerotic lesions. In our study, we found an almost perfect correlation between SUV_{max} calculated from the ROI including both vessel wall

and lumen compared to a ROI including only the vessel wall (**Figure 2**). This result indicates that the pixel in the PET image with the highest SUV is indeed located in the vessel wall in 96% of the slices and in the lumen in only 4%. This is not surprising since we acquire the PET/MR two hours after FDG injection, and we have previously shown a very low ^{18}F-FDG concentration in the blood three hours after injection [21]. More surprisingly, we also find a very strong correlation between SUV_{mean} with and without the vessel lumen included in the ROI. Since blood has low concentration of ^{18}F-FDG in relation to the vessel wall at the time of the PET acquisition, we would have expected a more pronounced increase in SUV_{mean} when excluding the lumen from the ROI. The reason for this observation is probably the resolution of the PET scanner and consequently a spill-over from the vessel wall to the lumen. Based on our results it seem appropriate to use the less time-consuming method of ROIs including both vessel wall and lumen for SUV calculations in patients without large plaques since the exclusion of the lumen is cumbersome and it will only change the values minimally. This conclusion could however be changed when point spread function is included in the reconstruction algorithm of the PET/MR system and perhaps by applying MR-based partial volume correction to the images [23].

Although the results of our feasibility study are promising, the findings are limited by the lack of large atherosclerotic plaques in the included patients. The aim of the present study was to compare the two imaging modalities in patients with increased risk of atherosclerosis but without identified carotid atherosclerosis. The results from ongoing studies will determine if our results can be extended to patients with large carotid plaques and high ^{18}F-FDG uptake.

Also, patients were moved from the PET/MR to the PET/CT scanner and despite meticulous coregistration a small misalignment between CT and MR on the slice by slice comparisons cannot be excluded, but in support of our data we find similar result in the vessel by vessel comparison. In addition, some intrascan patient movement may have occurred during the 30 min PET/MR acquisition despite the use of straps to fixate the head and neck. This would potentially lead to some decrease of the PET resolution.

Conclusion

In this first clinical study of simultaneous PET/MR for carotid artery imaging we found the method feasible in patients without large atherosclerotic plaques. Compared with PET/CT it yields comparable ^{18}F-FDG quantification and superior delineation of the vessel wall. Our study suggests that simultaneous PET/MR imaging of atherosclerosis should be studied further, especially in combination with functional MR imaging techniques.

Acknowledgements

The generous support from the John & Birthe Meyer Foundation, the National Advanced Technology Foundation, Danish Medical Research Council, Rigshospitalets Research Foundation, Svend Andersen Foundation, AP Møller Foundation, Novo Nordisk Foundation and Lundbeck Foundation is gratefully acknowledged. All of the staff in the PET center are thanked for their skillful technical assistance.

Address correspondence to: Dr. Andreas Kjær, Department of Clinical Physiology, Nuclear Medicine & PET, KF-4012 Rigshospitalet, Blegdamsvej 9, DK-2100 Copenhagen, Denmark. E-mail: akjaer@sund.ku.dk

References

[1] Graebe M, Pedersen SF, Borgwardt L, Hojgaard L, Sillesen H and Kjaer A. Molecular pathology in vulnerable carotid plaques: correlation with [18]-fluorodeoxyglucose positron emission tomography (FDG-PET). Eur J Vasc Endovasc Surg 2009; 37: 714-721.

[2] Pedersen SF, Graebe M, Fisker Hag AM, Hojgaard L, Sillesen H and Kjaer A. Gene expression and 18FDG uptake in atherosclerotic carotid plaques. Nucl Med Commun 2010; 31: 423-429.

[3] Cai JM, Hatsukami TS, Ferguson MS, Small R, Polissar NL and Yuan C. Classification of human carotid atherosclerotic lesions with in vivo multicontrast magnetic resonance imaging. Circulation 2002; 106: 1368-1373.

[4] Hatsukami TS, Ross R, Polissar NL and Yuan C. Visualization of fibrous cap thickness and rupture in human atherosclerotic carotid plaque in vivo with high-resolution magnetic resonance imaging. Circulation 2000; 102: 959-964.

[5] Subramanian S, Tawakol A, Burdo TH, Abbara S, Wei J, Vijayakumar J, Corsini E, Abdelbaky A, Zanni MV, Hoffmann U, Williams KC, Lo J and

Grinspoon SK. Arterial inflammation in patients with HIV. JAMA 2012; 308: 379-386.
[6] Yarasheski KE, Laciny E, Overton ET, Reeds DN, Harrod M, Baldwin S and Davila-Roman VG. 18FDG PET-CT imaging detects arterial inflammation and early atherosclerosis in HIV-infected adults with cardiovascular disease risk factors. J Inflamm (Lond) 2012; 9: 26
[7] Silvera SS, Aidi HE, Rudd JH, Mani V, Yang L, Farkouh M, Fuster V and Fayad ZA. Multimodality imaging of atherosclerotic plaque activity and composition using FDG-PET/CT and MRI in carotid and femoral arteries. Atherosclerosis 2009; 207: 139-143.
[8] Drzezga A, Souvatzoglou M, Eiber M, Beer AJ, Furst S, Martinez-Moller A, Nekolla SG, Ziegler S, Ganter C, Rummeny EJ and Schwaiger M. First Clinical Experience with Integrated Whole-Body PET/MR: Comparison to PET/CT in Patients with Oncologic Diagnoses. J Nucl Med 2012; 53: 845-855.
[9] Wiesmuller M, Quick HH, Navalpakkam B, Lell MM, Uder M, Ritt P, Schmidt D, Beck M, Kuwert T and von Gall CC. Comparison of lesion detection and quantitation of tracer uptake between PET from a simultaneously acquiring whole-body PET/MR hybrid scanner and PET from PET/CT. Eur J Nucl Med Mol Imaging 2013; 40: 12-21.
[10] Delso G, Furst S, Jakoby B, Ladebeck R, Ganter C, Nekolla SG, Schwaiger M and Ziegler SI. Performance measurements of the Siemens mMR integrated whole-body PET/MR scanner. J Nucl Med 2011; 52: 1914-1922.
[11] Martinez-Moller A, Souvatzoglou M, Delso G, Bundschuh RA, Chefd'hotel C, Ziegler SI, Navab N, Schwaiger M and Nekolla SG. Tissue classification as a potential approach for attenuation correction in whole-body PET/MRI: evaluation with PET/CT data. J Nucl Med 2009; 50: 520-526.
[12] Bland JM and Altman DG. Measuring agreement in method comparison studies. Stat Methods Med Res 1999; 8: 135-160.
[13] Okane K, Ibaraki M, Toyoshima H, Sugawara S, Takahashi K, Miura S, Shimosegawa E, Satomi J, Kitamura K and Satoh T. 18F-FDG accumulation in atherosclerosis: use of CT and MR coregistration of thoracic and carotid arteries. Eur J Nucl Med Mol Imaging 2006; 33: 589-594.
[14] Kwee RM, Teule GJ, van Oostenbrugge RJ, Mess WH, Prins MH, van der Geest RJ, Ter Berg JW, Franke CL, Korten AG, Meems BJ, Hofman PA, van Engelshoven JM, Wildberger JE and Kooi ME. Multimodality imaging of carotid artery plaques: 18F-fluoro-2-deoxyglucose positron emission tomography, computed tomography, and magnetic resonance imaging. Stroke 2009; 40: 3718-3724.
[15] Zaidi H, Ojha N, Morich M, Griesmer J, Hu Z, Maniawski P, Ratib O, Izquierdo-Garcia D, Fayad ZA and Shao L. Design and performance evaluation of a whole-body Ingenuity TF PET-MRI system. Phys Med Biol 2011; 56: 3091-3106.
[16] Keller SH, Holm S, Hansen AE, Sattler B, Andersen F, Klausen TL, Hojgaard L, Kjaer A and Beyer T. Image artifacts from MR-based attenuation correction in clinical, whole-body PET/MRI. MAGMA 2013; 26: 173-181.
[17] Samarin A, Burger C, Wollenweber SD, Crook DW, Burger IA, Schmid DT, von Schulthess GK and Kuhn FP. PET/MR imaging of bone lesions--implications for PET quantification from imperfect attenuation correction. Eur J Nucl Med Mol Imaging 2012; 39: 1154-1160.
[18] Hofmann M, Bezrukov I, Mantlik F, Aschoff P, Steinke F, Beyer T, Pichler BJ and Scholkopf B. MRI-based attenuation correction for whole-body PET/MRI: quantitative evaluation of segmentation- and atlas-based methods. J Nucl Med 2011; 52: 1392-1399.
[19] Bezrukov I, Mantlik F, Schmidt H, Scholkopf B and Pichler BJ. MR-Based PET attenuation correction for PET/MR imaging. Semin Nucl Med 2013; 43: 45-59.
[20] Johansson A, Karlsson M and Nyholm T. CT substitute derived from MRI sequences with ultrashort echo time. Med Phys 2011; 38: 2708-2714.
[21] Graebe M, Borgwardt L, Hojgaard L, Sillesen H and Kjaer A. When to image carotid plaque inflammation with FDG PET/CT. Nucl Med Commun 2010; 31: 773-779.
[22] Adams MC, Turkington TG, Wilson JM and Wong TZ. A systematic review of the factors affecting accuracy of SUV measurements. AJR Am J Roentgenol 2010; 195: 310-320.
[23] Wang H and Fei B. An MR image-guided, voxel-based partial volume correction method for PET images. Med Phys 2012; 39: 179-195.